Boletim da Sociedade Astronômica Brasileira, **34**, no. 1, 71-75

Testing the link between mergers and AGN in the Arp 245 system

Lösch, Elismar[1,2], Ruschel-Dutra, Daniel[2], Hernandez-Jimenez, Jose A.[3], & Rodrigues, Irapuan[3]

[1] Instituto de Astronomia, Geofísica e Ciências Atmosféricas, IAG-USP; e-mail: elismar.l@usp.br,
[2] Departamento de Física - Centro de Ciências Físicas e Matemáticas - Universidade Federal de Santa Catarina, CFM-UFSC,
[3] Instituto de Pesquisa & Desenvolvimento, Universidade do Vale do Paraíba (Univap)

Abstract. Mergers are decisive processes which occur frequently during the evolution of galaxies and may be correlated with extreme phenomena such as starbursts and active galactic nuclei (AGN). In order to investigate the influence of mergers on the nuclear activity, we performed a case study of the interacting system Arp 245, which hosts the active spiral NGC 2992 together with spiral NGC 2993. We employ hydrodynamical numerical simulations to reproduce and study the merger. The initial conditions of the simulations are built from photometric and kinematic analysis of the galaxies. A set of possible orbits for the system was also calculated considering observational positions and radial velocities of the galaxies as constraints. Here, we present and discuss two simulations which best reproduce the observed tidal features and velocity field of Arp 245.

Resumo. Mergers são processos decisivos que ocorrem com frequência durante a evolução de galáxias e que podem estar correlacionados com fenômenos extremos como surtos de formação estelar e núcleos ativos de galáxias (AGNs). De forma a investigar a influência dos mergers sobre a atividade nuclear, realizamos um estudo de caso do sistema em interação Arp 245, que abriga a galáxia espiral NGC 2992 juntamente com a espiral NGC 2993. Empregamos simulações numéricas hidrodinâmicas para reproduzir e estudar o merger. As condições iniciais das simulações foram construídas a partir de análises fotométricas e cinemáticas das galáxias. Um conjunto de possíveis órbitas para o sistema também foi calculado considerando-se posições e velocidades radiais das galáxias como vínculos. Aqui, apresentamos e discutimos duas simulações que melhor reproduzem as características de maré e campo de velocidade do Arp 245.

Keywords. Galaxies: interactions – Galaxies: active– Methods: numerical

1. Introduction

Mergers are some of the more disruptive processes that can occur during the evolution of a galaxy, and are one of key processes predicted by the ΛCDM cosmology, in which smaller structures merge to form larger ones (bottom-up scenario) (e.g. White and Rees (1978), Springel et al. (2005)). Furthermore, mergers are among the mechanisms that can cause a flux of gas to the center of galaxies, resulting in phenomena such as starbursts and active galactic nuclei (AGN) (e.g. Mihos and Hernquist (1994), Di Matteo et al. (2005), Guolo-Pereira et al. (2021)). Such processes can cause the exhaustion of gas in the galaxies, resulting in a gas-poor remnant galaxy (e.g. Springel et al. (2005), Hopkins et al. (2010)).

Despite the undeniable role of mergers in the evolution of galaxies, several uncertainties still surround the discussion. One of them are about the influence of mergers over AGN. It is a paradigm today in astrophysics that the vast majority of galaxies with masses greater than $\sim 10^{11} M_{\odot}$ hold a supermassive black hole (SMBH) in their centers (Kormendy and Ho (2013)). When fed with gas coming from the different regions of the galaxy, these objects can give rise to an AGN (Hopkins and Quataert (2010), Blumenthal and Barnes (2018)), objects with great mass-to-energy conversion efficiency whose luminosity can surpass that of the host galaxy itself. As already discussed, one of the mechanisms that can fed SMBHs with gas are mergers. However, secular processes such as bars (Regan and Teuben 2004), galaxy disk instabilities (Bournaud et al. 2011) and cosmological fluxes of gas (Feng et al. 2014) can also trigger AGNs, putting into dispute which type of process is more prevalent in giving rise to nuclear activity in different scenarios.

To understand which properties of galaxies can be explained or not by the occurrence of a major mergers is primordial to advance the knowledge about how the evolution of galaxies unfolds through cosmological time. This involves the comprehension of the history of star formation in galaxies, the growth of SMBHs, the exhaustion of gas in these galaxies, morphological changes through time, etc.

To study in detail the influence of a major merger over the nuclear activity of one of the galaxies involved, we performed a case study of the pair of galaxies Arp 245. Arp 245 is a system in interaction formed by the spiral galaxies NGC 2992 and NGC 2993, in addition to the dwarf galaxy Arp 245N. Through hydrodynamical simulations, Duc et al. (2000) reported that the system is in an early stage of the interaction, with the perigalacticon having taken place around $\approx$ 100 Myr ago. Several traces of the interaction can be observed in the system, specially the presence of tidal tails extending far beyond the galactic disks.

The system is most widely studied due to the nuclear activity observed in the NGC 2992 galaxy (e.g. Guolo-Pereira et al. (2021)). Optical spectroscopic observations have shown that NGC 2992 can be classified as a Seyfert, having already passed by the classifications of Seyfert 1.9, Seyfert 2.0 and, more recently, Schnorr-Müller et al. (2016) classified the galaxy as a Seyfert 1.8.

Taking into account that the galaxies are still relatively little affected by the merging process, and also considering the presence of an AGN in one of them, the system Arp 245 turns out to be an ideal target for our study, in which one of our main goal is to determine how the nuclear activity in NGC 2992 was affected by the merger. We also intend to understand the influence of the merger over other properties of the galaxies, such as their star formation rates and morphologies. For that we try to reproduce the system through N-body numerical simulations with the code GADGET-3, which includes astrophysical recipes for star formation and radiative cooling. We built the initial conditions of the

simulations based on observational constraints of the system, including photometric and kinematic data of the galaxies. A set of possible orbits for the interaction were also built based on observational inputs.

This paper is organized in two main sections. In section 2, we describe how the initial condition of the simulations were built, from the morphological models of the galaxies to the orbital parameters needed to run the merger. In section 3, we present our preliminary results regarding the simulations, and a brief discussion of what we obtained.

2. Building initial conditions

The first step to run numerical simulations of the Arp 245 system is to build its initial condition. This work can be divided in two main parts: to establish an adequate morphological description of the galaxies, and to obtain an orbit for the system that reproduces the system properly. In this section, we describe this process of obtaining the initial conditions of the system.

2.1. Density profiles

Regarding the density profiles of the galaxies, we assume they consist of four structural components: a dark matter halo, a stellar bulge, an exponential stellar disk, and a disk of gas divided in two parts: an exponential disk - similar to the stellar disk -, and an additional extended disk with constant radial and vertical density. We also include a central supermassive black hole.

The galaxies are build using the `MakeNewDisk` code, which implements the approach described in detail by Springel and White (1999) and Springel et al. (2005). In summary, we have the following density profiles for the structural components. The dark matter halos follow a Hernquist (1990) profile, i.e.

$$\rho_{dm}(r) = \frac{M_{dm}}{2\pi}\frac{a}{r(r+a)^3} \tag{1}$$

with cumulative mass profile $M(< r) = M_{dm}r^2/(r+a)^2$. Here, M_{dm} is the total mass and a is the scale length of the of the galaxy's dark matter halo, respectively. The preference for the Hernquist (1990) profile over the NFW profile (Navarro et al. 1996) is justified mainly by the faster decline in the outer parts of the halo in the case of the Hernquist (1990) profile, causing the total mass to converge and allowing the construction of isolated halos without the need for an ad-hoc truncation, which is not the case for the NFW profile.

Next, we have the stellar bulge, which, for simplicity, is taken to be spherical, and also following a Hernquist (1990) profile:

$$\rho_b(r) = \frac{M_b}{2\pi}\frac{b}{r(r+b)^3} \tag{2}$$

Similar to the dark matter halo, M_b here is the total mass of the galaxy's bulge, written as $M_b = m_b M_{tot}$, where M_{tot} is total mass of the galaxy, while b is the scale length of the bulge, expressed in units of the disk scale length.

The stellar and gas disk components are described with exponential surface density profiles, both with a scale length h:

$$\Sigma_{gas}(r) = \frac{M_{gas}}{2\pi h^2}\exp(-r/h) \tag{3}$$

$$\Sigma_{*}(r) = \frac{M_{*}}{2\pi h^2}\exp(-r/h) \tag{4}$$

where M_{gas} and M_* are the total mass of the (exponential) gas and stellar disks, respectively, and such that $M_d = (M_{gas} + M_d) = m_d M_{tot}$ is the total mass of the disk.

The vertical structure of the disk is given in terms of an isothermal sheet with radially constant vertical scale length z_0, so that the 3D stellar density profile in the disk is given by

$$\rho_*(R,z) = \frac{M_*}{4\pi z_0 h^2} sech^2\left(\frac{z}{2z_0}\right)\exp\left(-\frac{R}{h}\right) \tag{5}$$

In our model galaxies, we set the vertical scale length of stellar disks as $z_0 = 0.2h$.

The gas disk, on its turn, cannot be described in terms of a free parameter z_0, because once we take radiative cooling and star formation processes into account, we cannot choose the temperature freely, which would be necessary to define a z_0 for the gas. In this sense, the vertical scale of the gas disk will be "naturally" settled by such processes during the simulation.

Finally, the flat, extended gas disk is determined such that its mass is $M_{gas,c} = m_{gas,c}M_{gas}$ and its radial scale length is $h_{gas,c} = fh$, where $m_{gas,c}$ and f are the factors by which we multiply the total gas mass M_{gas} and radial scale length h to obtain the mass and scale length of this extended gas component.

2.2. Photometric and kinematic analysis

We applied the methodology described in Hernandez-Jimenez et al. (2013) and Hernandez-Jimenez et al. (2015) in order to analyze the photometry, kinematics and dynamics of the interacting galaxies of the Arp 245 system and obtain the paratemers necessary to build the galaxies using the morphological profiles described in the previous subsection.

In summary, the method consists of four steps. Starting with the surface brightness profile of the galaxies in a given band, we first need to symmetrize the image, so that any tidal features and other non-symmetric structures of the galaxies that may interfere with the subsequent analysis are removed. For that, we use a symmetrization method based on the m-fold concept to separate both symmetric and non-symmetric parts of the spiral pattern, by performing successive image rotations and subtractions (see Elmegreen et al. (1992)).

Next, the inverse Abel's integral is applied over the symmetrized images in order to de-project the brightness profile and obtain its form in three dimensions. Over the de-projected images, we finally obtain the density profiles for the different components of the galaxies. The third step then consists of obtaining the potential function of each component. This follows naturally from the previous step, once the density profiles and the potential functions are directly linked. The last step also follows naturally: to obtain the velocity fields of each component, which can be done by means of the Poisson Equation applied on the potential functions.

We applied Two Micron All Sky Survey (2MASS) H-band images of NGC 2992 and NGC 2993 to perform their photometric analysis. The observed velocity curve of NGC 2992, obtained from a Multi Unit Spectroscopic Explorer (MUSE) observation of the galaxy was also used to better constrain its kinematic analysis. The results for the density profiles and for the velocity curves of the galaxies are shown in figures 1 and 2, respectively. From the photometric analysis (density profiles), we can derive most of the parameters needed to build both the stellar disc and the stellar bulges (their total masses and radial scale lengths). Parameters such as total galaxy masses (M_{200}), halo concentration (c) and virial velocity (V_{200}) are derived from the kinematic analysis (velocity curves). The spin parameters (λ) were set as

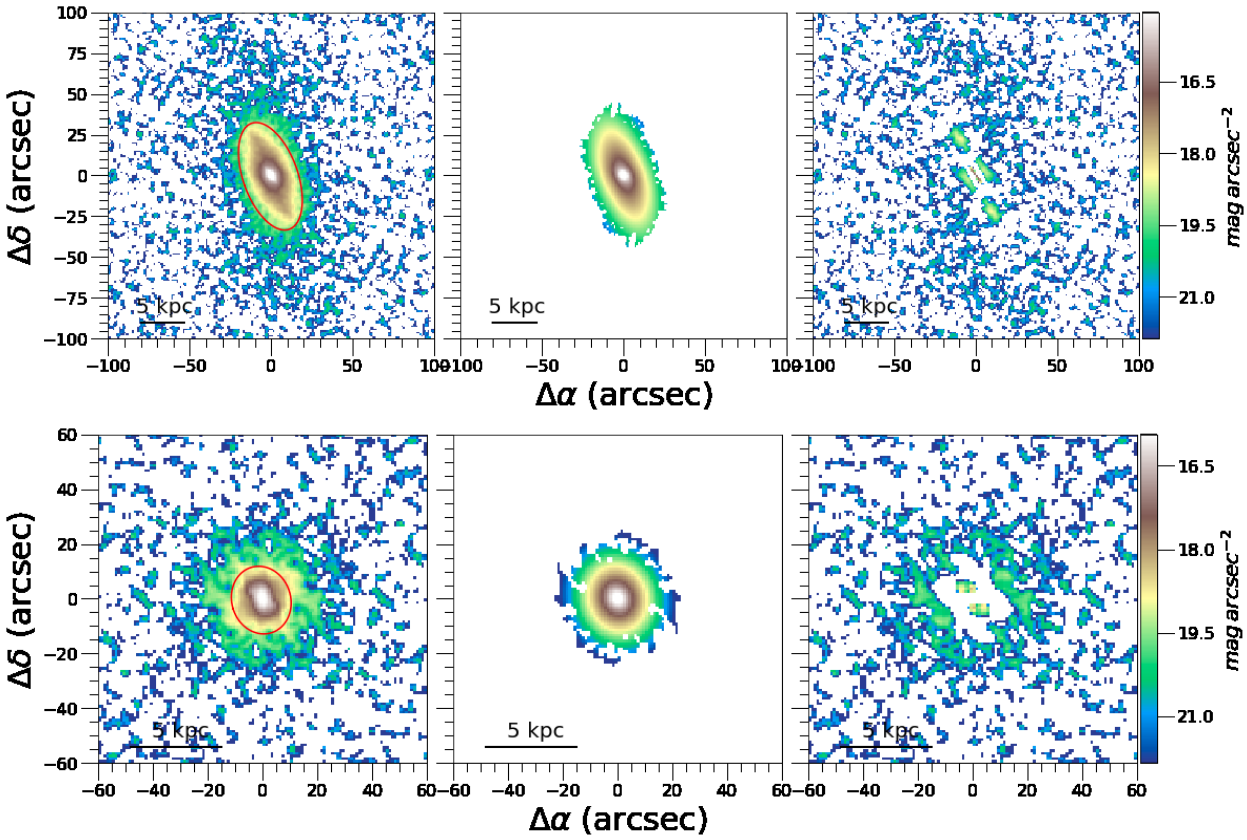

FIGURE 1: Luminosity density profile fit for NGC 2992 (top) and NGC 2993 (bottom). The leftmost panel shows the symmetrized image of the galaxies, the middle panel shows the best fit for each galaxy, and the rightmost panel shows the residuals of the fit.

the default value of 0.05, typical for halos in N-body simulations (Springel and White 1999). The same applies for the disk spin fractions, which were set as equal to the disk mass fractions. Finally, the black hole mass fraction (m_{bh}) was derived from the NGC 2992 SMBH mass obtained by Guolo-Pereira et al. (2021).

A summary of the parameters obtained for NGC 2992 and NGC 2993 is given in table 1.

2.3. Orbital parameters

Another crucial step to properly construct a model of the merger is the determination of the orbital parameters of the galaxies. The challenge here is that, in the study of interacting galaxies, observational constraints are insufficient to fully determine their orbits. Observations provide just 3 out of 6 phase-space coordinates: the projected position in the sky (X and Y), and the radial velocities (V_z) of the galaxies. The remaining 3 coordinates (Z, V_x and V_y) must the figured out.

The approach we applied to engender a set of possible orbits for the galaxies in the Arp 245 system consists of an algorithm which takes as input the observed X, Y, the relative radial velocity V_{sys} of the galaxies and its uncertainty $\sigma_{V_{sys}}$, the masses M and m of the main and secondary galaxies respectively, the unitary spin vector of the main disk galaxy of the system (in our case, NGC 2992) $\hat{s}$, a set of possible values for the orbit eccentricity, e, and a set of possible values for the orbit pericenter, q. The algorithm then calculates all orbits within this parameter space, and give as output the ones obeying the available observational constraints.

From that, a set of thousands of orbits is generated, which must then be tested to assess the ones which can better describe the observed system. Fortunately, groups of similar orbits are very common, and effectively just one from each of such groups needs to the tested in a simulation.

In table 2, we show the parameters of two orbits which turned out to produce the simulations that best match the observed features of Arp 245.

3. Preliminary results and discussion

In figure 3, we show the snapshots of these two simulations that best reproduced the observed morphological features in the galaxies of the Arp 245 system (figure 4).

We judged the simulations based on how well they were able to match observed features such as: i) the tidal arm of NGC 2992, which extends northwards; ii) the tidal arm of NGC 2993, extending eastwards; iii) the bridge of gas connecting the galaxies; iv) the bridge of stars connecting the galaxies; v) the relative sizes and positions of the galaxies; vi) the velocity field of the galaxies.

Comparing the snapshots of the simulations in figure 3 with the observed galaxies in figure 4, we can see that the simulation are able to reproduce relatively well at least the features i, ii and v. The biggest challenge we faced is regarding the bridge of gas and stars. These two features are present in several simulations we run, but they often appear exactly in simulations that are not able to develop the tidal arms of the galaxies. In spite of that, we can see the tentative formation of a bridge of stars and gas in the simulations of figure 3.

Finally, considering the velocity field of the galaxies, presented in figure 5, we see that in general there is a good match between our simulations and the observed velocity map of Arp

Parameter	NGC2992	NGC2993	Description
c	6.7	14.1	Halo concentration
V_{200} (km s^{-1})	182.0	120.0	Virial velocity
λ	0.05	0.05	Spin parameter
m_d	0.02029	0.02412	Disk mass fraction
m_b	0.00005	0.00122	Bulge mass fraction
m_{bh}	0.000024	0.0	Black hole mass fraction
j_d	0.00845	0.00870	Disk spin fraction
m_{gas}	0.428	0.428	Gas fraction in the disk
$z_0(m_d)$	0.2	0.2	Disk height
$b(m_d)$	0.181	0.267	Bulge scale length
$m_{gas,c}$	0.5	0.5	Mass fraction of extended gas disk
$h_{gas,c}$	6	6	Scale length of extended gas disk

TABLE 1: Morphological parameters used to build the numerical models of NGC 2992 and NGC 2993. The meaning of each parameter is described in the fourth column.

Orbit	e	q	r_{now}	v_q	X	Y	Z	V_x	V_y	V_z	s_x	s_y	s_z	Dir	ϕ_{SO}(°)	Peric
a	0.9	2	37.75	2714	-10.0	-15.0	-33.17	-36.20	112.3	-95.64	0.95	0.045	-0.31	Prograde	27.75	Pos
b	0.9	2	37.75	2714	-10.0	-15.0	-33.17	-59.58	109.2	-87.17	0.91	0.20	-0.37	Progade	18.16	Pos

TABLE 2: Orbital parameters of the simulations presented in figure 3. e) orbit excentricity; q) orbit distance of pericenter; r_{now}) current relative distance of the galaxies; v_q) orbit velocity of pericenter; X, Y, Z) X, Y and Z coordinates of secondary galaxy in the sky plane, respectively; V_x, V_y, V_z) x, y, and z components of the relative velocity of the galaxies in the sky plane, respectively; s_x, s_y, s_z) x, y, and z components of the unitary spin vector of the main galaxy disk; Dir) direction of the encounter (prograde or retrograde); ϕ_{SO}) angle between the spin vector s and the orbit spin vector; Peric) current situation of the merger: pre of post-pericenter.

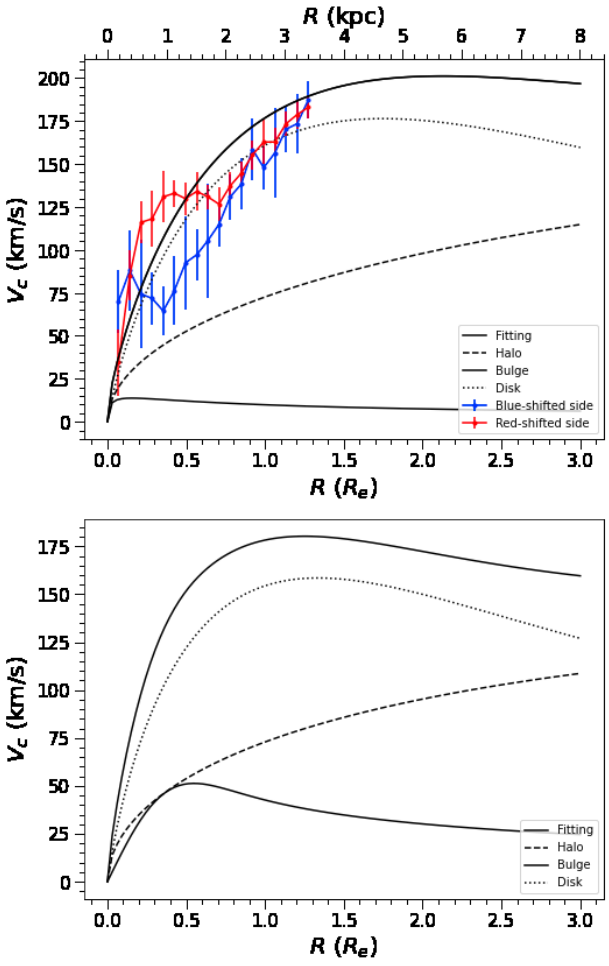

FIGURE 2: Rotation curves obtained for NGC 2992 (top) and NGC 2993 (bottom). The rotation curves for each component are shown separately, as well as the "total" rotation curve. In the case of NGC 2992, the observed rotation curve is also shown.

245. For instance, the tidal arm of NGC 2992 presents a velocity around 300 km s^{-1} in the simulations, which is similar to the observed value. The remaining regions of Arp 245 have velocities ranging from around −100 km s^{-1} to 200 km s^{-1} of higher, which is also observed in the simulations, except for some groups of particles which seem detached from the main bodies of the galaxies, having higher velocities.

In summary, our conclusions so far is that we were able to reasonably reproduce the merger in Arp 245, the only major remaining challenge being the lack of a proper bridge of gas and stars between the galaxies.

We also hope to do further analysis of the simulations regarding the inflow of gas to galactic centers, the star formation, the metallicity gradient and other properties of the galaxies that were probably affected the merging process, meeting the initial purpose of the project.

References

Blumenthal, K. A. and J. E. Barnes (2018, September). Go with the Flow: Understanding inflow mechanisms in galaxy collisions. *MNRAS 479*(3), 3952–3965.

Bournaud, F., A. Dekel, R. Teyssier, M. Cacciato, E. Daddi, S. Juneau, and F. Shankar (2011, November). Black Hole Growth and Active Galactic Nuclei Obscuration by Instability-driven Inflows in High-redshift Disk Galaxies Fed by Cold Streams. *ApJ 741*(2), L33.

Di Matteo, T., V. Springel, and L. Hernquist (2005, February). Energy input from quasars regulates the growth and activity of black holes and their host galaxies. *Nature 433*(7026), 604–607.

Duc, P. A., E. Brinks, V. Springel, et al. (2000, Sep). Formation of a Tidal Dwarf Galaxy in the Interacting System Arp 245 (NGC 2992/93). *ApJ 120*(3), 1238–1264.

Elmegreen, B. G., D. M. Elmegreen, and L. Montenegro (1992, March). Optical Tracers of Spiral Wave Resonances in Galaxies. II. Hidden Three-Arm Spirals in a Sample of 18 Galaxies. *ApJS 79*, 37.

Feng, Y., T. Di Matteo, R. Croft, and N. Khand ai (2014, May). High-redshift supermassive black holes: accretion through cold flows. *MNRAS 440*(2), 1865–1879.

Guolo-Pereira, M., D. Ruschel-Dutra, T. Storchi-Bergmann, A. Schnorr-Müller, R. Cid Fernandes, G. Couto, N. Dametto, and J. A. Hernandez-Jimenez (2021, April). Exploring the AGN-merger connection in Arp 245 I: Nuclear star formation and gas outflow in NGC 2992. *MNRAS 502*(3), 3618–3637.

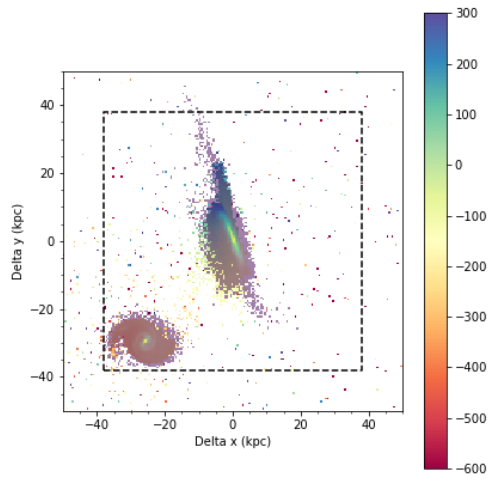

(a)

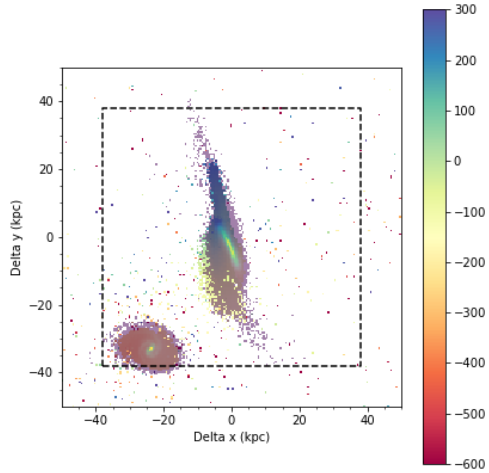

(b)

FIGURE 3: Representative snapshots of two of our best simulations of Arp 245. The colorbar represents the radial velocity of the galaxies in kms^{-1}, and is superposed by the density of stars.

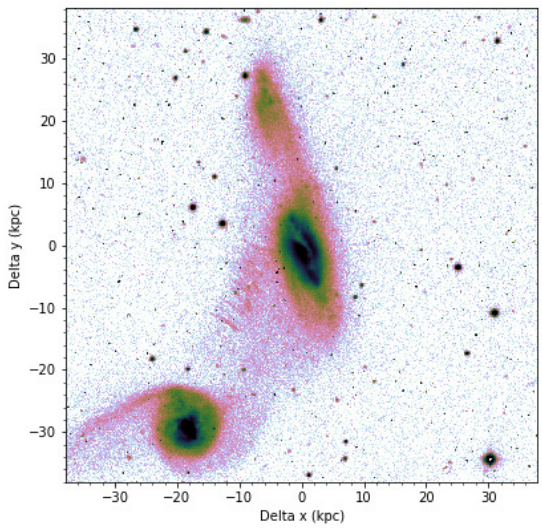

FIGURE 4: Observation of Arp 245 from the Cerro Tololo Inter-American Observatory (CTIO).

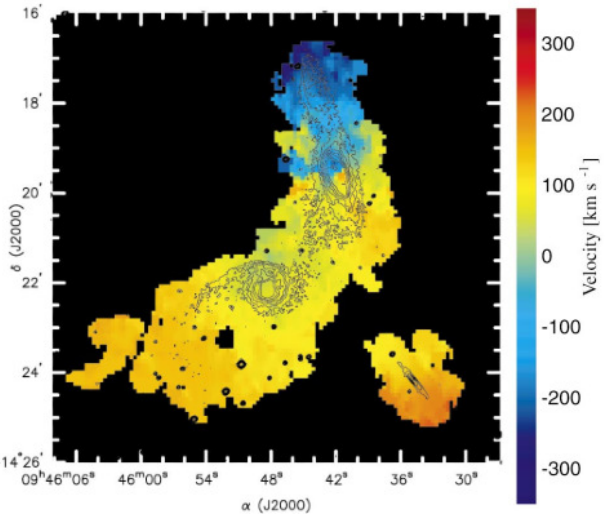

FIGURE 5: HI velocity map of Arp 245, with optical contours superposed. Extracted from Duc et al. (2000).

Hernandez-Jimenez, J. A., M. G. Pastoriza, C. Bonatto, I. Rodrigues, A. C. Krabbe, and C. Winge (2015, August). Photometry and dynamics of the minor mergers AM 1228-260 and AM 2058-381. *MNRAS 451*(3), 2278–2294.

Hernandez-Jimenez, J. A., M. G. Pastoriza, I. Rodrigues, A. C. Krabbe, C. Winge, and C. Bonatto (2013, November). Photometry and dynamics of the minor merger AM 1219-430 with Gemini GMOS-S. *MNRAS 435*(4), 3342–3352.

Hernquist, L. (1990, June). An Analytical Model for Spherical Galaxies and Bulges. *ApJ 356*, 359.

Hopkins, P. F., K. Bundy, D. Croton, L. Hernquist, D. Keres, S. Khochfar, K. Stewart, A. Wetzel, and J. D. Younger (2010, May). Mergers and Bulge Formation in ΛCDM: Which Mergers Matter? *ApJ 715*(1), 202–229.

Hopkins, P. F. and E. Quataert (2010, September). How do massive black holes get their gas? *MNRAS 407*(3), 1529–1564.

Kormendy, J. and L. C. Ho (2013, August). Coevolution (Or Not) of Supermassive Black Holes and Host Galaxies. *ARA&A 51*(1), 511–653.

Mihos, J. C. and L. Hernquist (1994, August). Ultraluminous Starbursts in Major Mergers. *ApJ 431*, L9.

Navarro, J. F., C. S. Frenk, and S. D. M. White (1996, May). The Structure of Cold Dark Matter Halos. *ApJ 462*, 563.

Regan, M. W. and P. J. Teuben (2004, January). Bar-driven Mass Inflow: How Bar Characteristics Affect the Inflow. *ApJ 600*(2), 595–612.

Schnorr-Müller, A., R. I. Davies, K. T. Korista, et al. (2016, November). Constraints on the broad-line region properties and extinction in local Seyferts. *MNRAS 462*(4), 3570–3590.

Springel, V., T. Di Matteo, and L. Hernquist (2005, February). Black Holes in Galaxy Mergers: The Formation of Red Elliptical Galaxies. *ApJ 620*(2), L79–L82.

Springel, V. and S. D. M. White (1999, July). Tidal tails in cold dark matter cosmologies. *MNRAS 307*(1), 162–178.

Springel, V., S. D. M. White, A. Jenkins, C. S. Frenk, N. Yoshida, L. Gao, J. Navarro, R. Thacker, D. Croton, J. Helly, J. A. Peacock, S. Cole, P. Thomas, H. Couchman, A. Evrard, J. Colberg, and F. Pearce (2005, June). Simulations of the formation, evolution and clustering of galaxies and quasars. *Nature 435*(7042), 629–636.

White, S. D. M. and M. J. Rees (1978, May). Core condensation in heavy halos: a two-stage theory for galaxy formation and clustering. *MNRAS 183*, 341–358.